

Self-polarization effect on large photovoltaic response in lead free ferroelectric $0.5\text{Ba}(\text{Zr}_{0.2}\text{Ti}_{0.8})\text{O}_3\text{-}0.5(\text{Ba}_{0.7}\text{Ca}_{0.3})\text{TiO}_3$ epitaxial film

Atal Bihari Swain, Martando Rath, Subhajit Pal, M. S. Ramachandra Rao, V. Subramanian, and P. Murugavel

Citation: *Appl. Phys. Lett.* **113**, 233902 (2018); doi: 10.1063/1.5068699

View online: <https://doi.org/10.1063/1.5068699>

View Table of Contents: <http://aip.scitation.org/toc/apl/113/23>

Published by the [American Institute of Physics](#)

Articles you may be interested in

[Understanding and predicting geometrical constraint ferroelectric charged domain walls in a \$\text{BiFeO}_3\$ island via phase-field simulations](#)

Applied Physics Letters **113**, 222902 (2018); 10.1063/1.5050802

[Polarization imprint effects on the photovoltaic effect in \$\text{Pb}\(\text{Zr,Ti}\)\text{O}_3\$ thin films](#)

Applied Physics Letters **112**, 152905 (2018); 10.1063/1.5020694

[Evolution from successive phase transitions to “morphotropic phase boundary” in \$\text{BaTiO}_3\$ -based ferroelectrics](#)

Applied Physics Letters **112**, 182903 (2018); 10.1063/1.5028302

[Integration of ferroelectric \$\text{Pb}\(\text{Zr}_{0.52}\text{Ti}_{0.48}\)\text{O}_3\$ thin films on conducting nanocrystalline diamond for high performance device applications](#)

Applied Physics Letters **113**, 032904 (2018); 10.1063/1.5035450

[Strain induced enhancement of erasable domain wall current in epitaxial \$\text{BiFeO}_3\$ thin films](#)

Journal of Applied Physics **124**, 194102 (2018); 10.1063/1.5054945

[Electric-field-controllable nonvolatile multilevel resistance switching of \$\text{Bi}_{0.93}\text{Sb}_{0.07}/\text{PMN-}0.29\text{PT}\(111\)\$ heterostructures](#)

Applied Physics Letters **113**, 223504 (2018); 10.1063/1.5049789



Lake Shore
CRYOTRONICS



Cryogenic probe stations
for accurate, repeatable
material measurements

LEARN MORE 

Self-polarization effect on large photovoltaic response in lead free ferroelectric $0.5\text{Ba}(\text{Zr}_{0.2}\text{Ti}_{0.8})\text{O}_3\text{-}0.5(\text{Ba}_{0.7}\text{Ca}_{0.3})\text{TiO}_3$ epitaxial film

Atal Bihari Swain,¹ Martando Rath,^{1,2} Subhajit Pal,¹ M. S. Ramachandra Rao,^{1,2} V. Subramanian,¹ and P. Murugavel^{1,a)}

¹Department of Physics, Indian Institute of Technology Madras, Chennai 600036, India

²Nano Functional Materials Technology Centre, Department of Physics, Indian Institute of Technology Madras, Chennai 600036, Tamil Nadu, India

(Received 18 October 2018; accepted 17 November 2018; published online 6 December 2018)

An epitaxial lead free ferroelectric $0.5\text{Ba}(\text{Zr}_{0.2}\text{Ti}_{0.8})\text{O}_3\text{-}0.5(\text{Ba}_{0.7}\text{Ca}_{0.3})\text{TiO}_3$ (BZT-BCT) thin film is fabricated on a (001)Nb:SrTiO₃ single crystalline substrate by the pulsed laser deposition method. The 2.3% lattice mismatch between the BZT-BCT and substrate suggests that the film is grown under a compressively strained state by leaving a large strain gradient near the interface. Polarization versus electric field measurement reveals that the film exhibits a ferroelectric hysteresis character with a large imprint effect indicating the existence of an internal electric field. The origin of the internal electric field is correlated with the strain gradient induced flexoelectric effect and the interfacial built-in field. Consequently, the resultant internal electric field could lead to a self-polarized non-switchable layer at the interface. The evidence for the envisaged self-polarization effect is indeed shown by the piezo force microscopic measurements. Importantly, photovoltaic studies performed on the film display an open circuit voltage of 1.1 V, which is higher than the values reported for many ferroelectric films. The observed photovoltaic response is correlated with the depolarization field and the self-polarization effect. The demonstrated large photo-response illustrates the application potential of the BZT-BCT system in photovoltaic devices.

Published by AIP Publishing. <https://doi.org/10.1063/1.5068699>

The spontaneous and switchable polarization of the ferroelectric materials facilitated their applications in non-volatile memory devices,^{1,2} tunnel junctions,^{3,4} resistive switching,⁵ etc. In addition, there is numerous research interest in extending their application potential in the field of energy harvesting by transforming the wide range of unconsumed energy sources such as vibrations, mechanical fluctuations, solar radiations, and temperature variation.⁶ Recently, the work on the photovoltaic (PV) effect on ferroelectric oxides is gaining momentum due to the above observed bandgap open-circuit voltage (V_{OC}).^{7,8} Such a large photo-response can make them an attractive candidate in the pursuit of alternative to the existing green energy conversion sources. Of late, several ferroelectric oxides were reported to exhibit interesting PV characteristics along with various diversified mechanisms for the observed above-bandgap ferroelectric photovoltage.^{9–11} However, the ferroelectric systems studied are limited to a selected few such as LiNbO₃,¹² BaTiO₃,¹³ $(\text{Pb}_{0.97}\text{La}_{0.03})(\text{Zr}_{0.52}\text{Ti}_{0.48})\text{O}_3$ (PLZT),¹⁴ BiFeO₃ (BFO),⁷ and $\text{Pb}(\text{Zr}_{1-x}\text{Ti}_x)\text{O}_3$ (PZT).¹⁵ In this regard, it is highly imperative to search for ferroelectrics exhibiting a large PV response so as to widen the available ferroelectric PV materials which will enable better understanding about the PV mechanism.

Interestingly, Poosanaas and Uchino¹⁴ proposed the empirical correlation between the photovoltage and morphotropic phase boundary (MPB) composition in a ferroelectric system. In this scenario, the recently discovered lead free ferroelectric $0.5\text{Ba}(\text{Zr}_{0.2}\text{Ti}_{0.8})\text{O}_3\text{-}0.5(\text{Ba}_{0.7}\text{Ca}_{0.3})\text{TiO}_3$ (BZT-BCT) system¹⁶ having an MPB composition can be considered as a

potential candidate to explore the PV effect. Importantly, it is one of the Pb-free alternatives owing to its large piezoelectric coefficient (d_{33}) value of ~ 620 pC/N. However, the physical characteristics of BZT-BCT thin films are limited in literature and notably, the PV properties are unexplored till date despite the compound exhibiting a PV favourable MPB composition.^{14,16} In this work, we have fabricated an epitaxial thin film of BZT-BCT on a 5% Nb doped (001)SrTiO₃ (Nb:STO) substrate by the pulsed laser deposition (PLD) technique and studied its ferroelectric properties along with the PV characteristics. The film showed a strong self-polarization effect and a remarkable PV response of 1.1 V as the open circuit voltage. The possible correlations between the self-polarization and large PV response are discussed in this letter. The results presented in this letter elucidate the significance of the BZT-BCT system in future PV and self-powered photodetector related applications.^{17,18}

To fabricate the BZT-BCT film by the PLD technique, the target was prepared by the solid state route. Initially, homogeneously mixed stoichiometric amounts of BaCO₃, CaCO₃, BaZrO₃, and TiO₂ precursors were calcined at 1350 °C for 4 h.¹⁹ The calcined powder was mixed with 6 wt. % polyvinyl alcohol as the binder and uniaxially pressed into a 12 mm diameter disc shaped pellet. The green pellet was sintered at 1450 °C for 6 h for better densification and used as the target. The film was deposited on the (001)Nb:STO substrate at 720 °C at 400 mTorr of oxygen partial pressure (PO₂). The deposition was carried out by ablating the target using excimer laser (10 Hz pulse frequency and 2.3 mJ/cm² fluence) for 15 min. After deposition, the film was annealed *in-situ* under 500 Torr of PO₂ for 30 min, then cooled to

^{a)}Author to whom correspondence should be addressed: muruga@iitm.ac.in

room temperature at 10 °C/min. For better crystallinity, the grown film was again annealed *ex-situ* at 850 °C for 1 h under an ambient condition.

The fabricated film was analysed by the X-ray diffraction (XRD) technique (Rigaku with Ni filter and Cu K_α radiation) for its crystalline phase and orientation. Surface profilometry (Bruker Contour GT-3d) was used to verify the thickness homogeneity of the film. The optical bandgap was measured by diffuse reflectance spectroscopy (DRS) using a micropack DH2000 lamp (deuterium in UV-vis and Halogen in vis-NIR). For electrical measurements, 200 μm diameter thin Au dots were deposited as top electrodes, whereas the conducting Nb:STO substrate was used as the bottom electrode. The ferroelectric polarization (P) versus electric field (E) measurements were performed in the Au/BZT-BCT/Nb:STO capacitor geometry using a Radiant Technology instrument (USA RT6000S). Piezo force microscopy (Parks System XE, South Korea) was used for the ferroelectric switching characteristics, where the conducting Au tip of 75 kHz resonant frequency and 2.5 N/m force constant were used. The photovoltaic measurements were carried out using a Keithley high resistance electrometer (6517B) with a Xenon arc lamp as the light source.

The θ - 2θ XRD pattern recorded on the film is shown in Fig. 1(a) and the pattern reveals the formation of the film without any secondary phases. The XRD pattern displays the diffraction peaks corresponding to the (00 l) plane of the tetragonal phase revealing the c -axis orientation of the BZT-BCT film. To confirm the degree of orientation, the ϕ -scan is performed on (111) diffraction peaks of both the film and substrate. The results are displayed in Fig. 1(b). The perfect match in the diffraction peaks of the film with the substrate

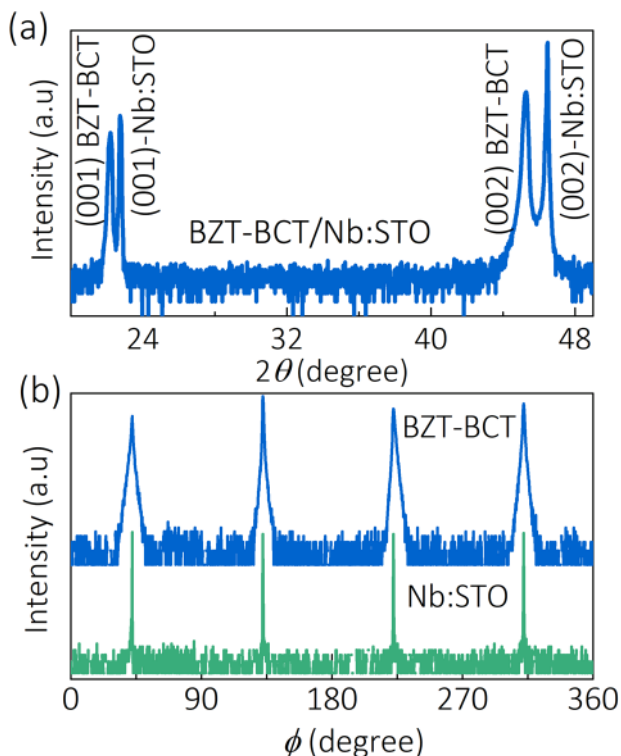


FIG. 1. (a) XRD θ - 2θ pattern of the BZT-BCT/Nb:STO film and (b) ϕ -scan of Nb:STO and BZT-BCT at (111) diffraction peaks.

and their repetition at 90° interval indicate one-on-one growth with the in-plane 4-fold rotational symmetry of the film. This confirms that the film is epitaxially grown along the (00 l) orientation. The lattice parameters of the bulk BZT-BCT sample are $a = 3.9986 \text{ \AA}$ and $c = 4.0192 \text{ \AA}$,^{20,21} whereas the cubic Nb:STO lattice parameter (a_{subs}) = 3.905 \AA . Hence, the c -axis oriented epitaxial film is expected to grow under a compressively strained condition with 2.3% ($[(a_{\text{subs}} - a)/a] \times 100$) misfit strain.^{21,22}

The topography of the as-grown film recorded by piezo force microscopy (PFM) (see [supplementary material S1](#)) shows a smooth surface with an average surface roughness of $\sim 5 \text{ nm}$. The thickness homogeneity of the film is evidenced from the uniform colour contrast shown by the surface profilometry image in Fig. 2(a) and the thickness calculated from the image is $\sim 335 \text{ nm}$ (see [supplementary material S2](#)). The optical reflectance (R) spectrum of the film shown in the inset of Fig. 2(b) reveals a sharp absorption below the visible wavelength range which indicates that the bandgap of BZT-BCT is in the UV absorption range. The bandgap of the film obtained from the Kubelka-Munk (K-M) plot,²³ which is the plot of $(F(R)h\nu)^{1/2}$ versus energy, where $F(R) = (1 - R)^2/2R$, drawn in Fig. 2(b), is 3.18 eV.

To ascertain the ferroelectric properties, P - E hysteresis loop measurements are carried out on the Au/BZT-BCT/Nb:STO film at 50 Hz. The evolution of the P - E loops showing ferroelectric characteristics at various applied voltages is shown in Fig. 2(c). Interestingly, the loops exhibit polarization imprint with a large voltage off-set suggesting the presence of an in-built internal electric field (E_{in}) in the system.²⁴⁻²⁸ The P - E loops display large asymmetry in remnant polarization (P_r) with $+P_r = -0.8$ and $-P_r = -6.5 \mu\text{C}/\text{cm}^2$. The large imprint is generally attributed to the non-switchable layer at the film interface.^{22,25,26} The origin for such non-switching layer is correlated with the strain gradient and domain pinning at the interface in the literature.^{21,22,24-28} Note that the BZT-BCT film is grown on the Nb:STO substrate under 2.3% compressive strain. During the epitaxial growth process, the unit cells are grown layer by layer on the substrate. However, the layers start relaxing as it grows from the interface to the bulk direction leaving a

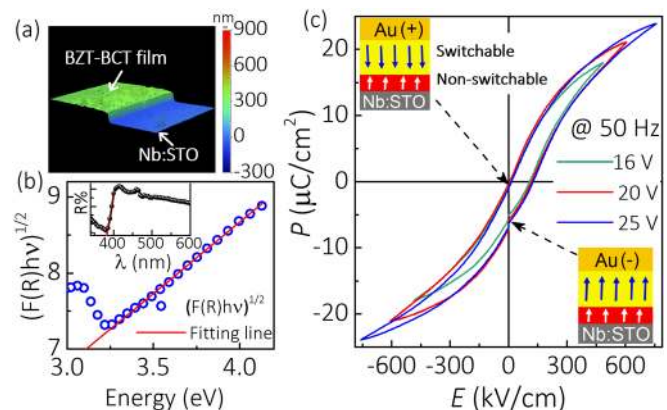


FIG. 2. (a) Surface profilometry image, (b) K-M plot, and (c) P - E hysteresis loops of the BZT-BCT/Nb:STO film. The inset in the K-M plot shows the reflectance versus wavelength graph. The insets in the P - E loop show the schematic representations of switchable and non-switchable domains under the external electric field.

large strain gradient along the thickness of the film. The strain gradient can generate large flexoelectric field^{21,22,27–29} which in turn can cause a preferential orientation of polarization called the self-polarization over a small thickness range from the film-substrate interface as shown in the inset of Fig. 2(c).^{28,29}

In a simplified form, the strength of the self-polarization $P = \mu \frac{\partial u}{\partial z}$ induced by the flexoelectric field ($E_{\text{flex}} = \frac{e}{4\pi\epsilon_0 a} \frac{\partial u}{\partial z}$), where $\partial u/\partial z$ is the strain gradient, z is the distance from the film surface, e is the charge of an electron, a is the lattice parameter of the BZT-BCT compound, and ϵ_0 is the absolute permittivity, correlated with the flexoelectric coefficient μ .^{30,31} By considering the $\partial u/\partial z = u_m^2/a$, the calculated $\partial u/\partial z$ and E_{flex} are $\sim 1.32 \times 10^6 \text{ m}^{-1}$ and 4.75 MV m^{-1} , respectively.²² Note that the lattice misfit strain u_m is calculated from the lattice parameter of the BZT-BCT and the substrate.²² In addition, the induced self-polarization P which assumed to be $\sim P_r/2$ ($= 3.5 \mu\text{C}/\text{cm}^2$), gives an approximate estimation for $\mu \sim 2.651 \times 10^{-8} \text{ C m}^{-1}$ which is in fact much large than the values reported for other bulk ferroelectrics.²⁸ Moreover, to absorb the misfit strain, the approximate thickness of the non-switchable self-polarization layer (a/u_m) is $\sim 18 \text{ nm}$.²² These self-polarized domains are difficult to switch under a normal external field and thereby leave non-switchable domains at the interface as shown in the inset of Fig. 2(c).²² In addition, the n-type semiconducting Nb:STO substrate results in a p-n junction at the interface with the p-type ferroelectric film. As a consequence, the internal electric field (E_{in}) in the depletion region (pointing towards the thickness direction) can additionally favour a non-switchable upward polarization (domain pinning effect) at the film-substrate interface.²⁹ Hence, a large imprint observed in the BZT-BCT/Nb:STO film could be the combined effect of the strain gradient and domain pinning.

To further understand the domain switching, piezo force microscopic (PFM) measurements are carried out on the film. Initially, the domain pattern is written over $4 \times 4 \mu\text{m}^2$ with $+10 \text{ V}$ dc bias voltage followed by $2 \times 2 \mu\text{m}^2$ of central area written by -10 V dc bias voltage. The PFM signal is read by 1 V ac signal over $6 \times 6 \mu\text{m}^2$ area and the obtained amplitude and phase images are displayed in Figs. 3(a) and 3(b), respectively. The uniform colour contrast seen in Fig. 3(b) at the central $2 \times 2 \mu\text{m}^2$ area indicates that the domains are fully switched along the upward direction (away from the substrate). However, the area written by $+10 \text{ V}$ shows almost similar colour contrast with the as-grown sample (outer area), which indicates the difficulty in switching the domain in the downward direction. The observation reiterates the presence of non-switchable self-polarized upward domains. Hence, the resultant self-polarized field is in-phase and against the field applied to switch the domains in upward and downward directions, respectively. To investigate it further, the PFM amplitude (d_{33}) and phase curves are plotted in Figs. 3(c) and 3(d), respectively. The plots show a butterfly-like ferroelectric d_{33} curve along with the dynamic domain switching with a 180° phase shift. However, the strong imprint-like feature evidenced from the observed shift in the respective plots is attributed to the effect of the non-switchable layer at the interface. The evidence for the non-switchable domains and its effects on the ferroelectric imprint behaviour are reported in similar systems like PZT/Nb:STO thin films.²⁵

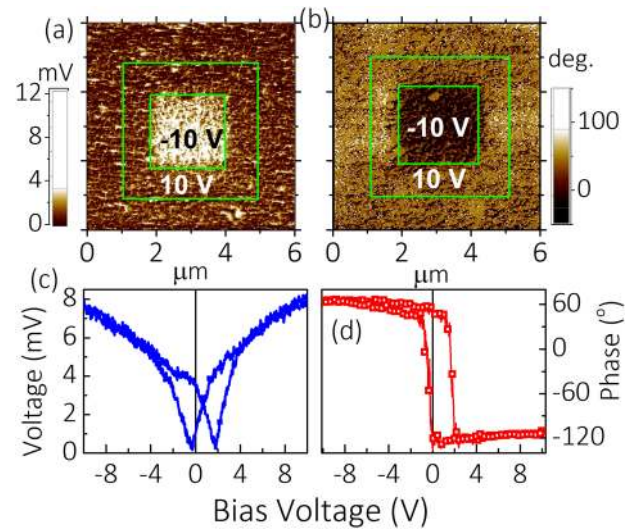


FIG. 3. The PFM (a) amplitude and (b) phase image of the $6 \times 6 \mu\text{m}^2$ BZT-BCT film read by the 1 V ac signal after writing the pattern over $4 \times 4 \mu\text{m}^2$ by $+10 \text{ V}$ and $2 \times 2 \mu\text{m}^2$ by -10 V dc voltage. The PFM (c) amplitude and (d) phase curves recorded on the BZT-BCT film.

The optical bandgap of the film being in the UV absorption range and ferroelectric polarization strongly suggest the suitability of the BZT-BCT film for PV studies. To probe the PV characteristic, the current versus voltage measurements are carried out on an Au/BZT-BCT/Nb:STO capacitor structure under dark and light illumination conditions. The schematic geometry used for PV measurement is shown in the inset of Fig. 4(a). Prior to the PV measurements, the sample is poled under -10 V dc voltage for 10 min . The Au and Nb:STO electrodes are connected to the negative and positive terminals, respectively, and the resultant polarization state is labelled as P_{up} state. The measured J - V curves are shown in Fig. 4(a). Notably, the BZT-BCT sample displays a strong PV response with a maximum V_{OC} of 1.1 V and a short-circuit current density (J_{sc}) of $\sim 2 \mu\text{A}/\text{cm}^2$ under $100 \text{ mW}/\text{cm}^2$ light intensity. The displayed V_{OC} and J_{sc} values are better than the values reported for the Pb-based ferroelectric films and even higher than the well-studied BiFeO₃ film.^{30–32} As a comparison, the J_{sc} and normalized V_{OC} with respect to the thickness (d) reported for the ferroelectric epitaxial films exhibiting a large PV response at $100 \text{ mW}/\text{cm}^2$ light intensity are given in Table I.

The table highlights the significance of the BZT-BCT system in PV studies. For the switchable PV effect, the measurements are repeated, but by applying $+10 \text{ V}$ as the poling voltage. The resultant polarization state is labelled as the P_{down} state. Ironically, the sample did not show any PV response under light illumination as shown in Fig. 4(a). This is in accordance with the presence of self-polarization induced non-switchable ferroelectric domains at the film-substrate interface which give rise to the imprint effect resulting in a very low remnant polarization ($+P_r = -0.8 \mu\text{C}/\text{cm}^2$) value.

In general, the PV effect is about the electron-hole pair generation followed by their separation and collection before recombination. In ferroelectric thin films, the separation of photo-generated electron-hole pairs is facilitated by the internal electric field.^{10,11} The following two mechanisms majorly contribute to the ferroelectric PV response via the

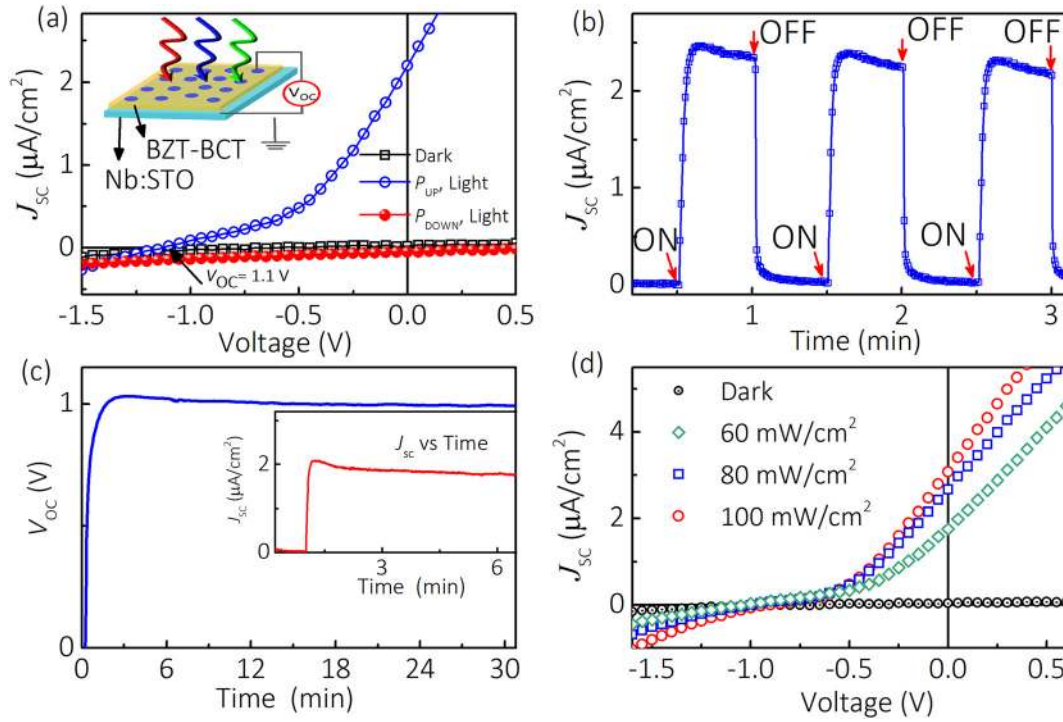


FIG. 4. (a) Photovoltaic J - V curves recorded under dark and light illumination (the inset is the schematic of PV measurement geometry), (b) transient photocurrent response under light ON and OFF states, (c) V_{OC} recorded as a function of time (the inset shows the J_{SC} versus time plot), and (d) J - V plots measured at different light intensities for the Au/BZT-BCT/Nb:STO heterostructure.

internal field. They are the polarization induced depolarization field (E_{dp}) and the built-in field (E_{bi}) due to the metal/ferroelectric Schottky barrier formation at the interface. Note that the E_{dp} originates due to incomplete screening of polarization induced surface bound charges, whose direction can be switched by changing the poling field direction. The net internal electric field (E_{net}) responsible for the charge separation is $E_{net} = E_{bi} \pm E_{dp}$.^{36,37} In addition, in BZT-BCT, the large PV response is also associated with the non-switchable self-polarization field (E_{sp}) whose direction is along and against the P_{up} and P_{down} states, respectively. Hence, the observed PV response in the P_{up} state and its absence in P_{down} states is the consequence of the related change in the net internal field ($E_{net} = E_{bi} \pm E_{dp} + E_{sp}$) dominated by E_{sp} .

To understand it better, we have drawn the energy band diagram of the heterostructure subjected to unpoled, P_{up} and P_{down} states in Figs. 5(a), 5(b), and 5(c), respectively. In an unpoled state, the difference in the work function (5.1 eV) and electron affinity ($\chi_e = 3.9$ eV) of Au and BZT-BCT,³⁸ respectively, yields the Schottky barrier at the top interface with the resultant barrier height ϕ_t of 1.2 eV (the corresponding

$E_{bi} = 3.6$ MV/m) and depletion width W_t as shown in Fig. 5(a). On the other hand, the χ_e of Nb:STO being 4.08 eV gives³⁹ a nominal barrier height of 0.18 eV (the corresponding $E_{bi} = 0.30$ MV/m) and depletion width W_b at the bottom interface as shown in Fig. 5(c). Hence, the band bending at the bottom interface is mostly dominated by E_{sp} which is along the direction of E_{bi} as shown in Fig. 5(a). However, in the P_{up} state, the direction of E_{dp} being along the direction of E_{sp} and E_{bi} , leads to an increase in the width of depletion regions (W_t and W_b) with an enhanced band bending at both interfaces as shown in Fig. 5(b). As a consequence, the increased $E_{net} (= E_{bi} + E_{dp} + E_{sp})$ favours better charge separation and hence higher V_{OC} and J_{SC} . On the other hand, in the P_{down} state the E_{dp} , which is now opposite to the direction of E_{sp} and E_{bi} , lowers the $E_{net} (= E_{bi} - E_{dp} + E_{sp})$ and reduces the band bending effect at both interfaces and even giving possible upward band bending as shown in Fig. 5(c). As a consequence, the lower E_{net} reduced the rate of photo-generated charge separation with an almost negligible PV response [shown in Fig. 4(a)] in the P_{down} state.

TABLE I. Comparison of reported J_{SC} and V_{OC}/d in epitaxial ferroelectric PV response along with the BZT-BCT system.

Epitaxial films	V_{OC}/d (kV/cm)	J_{SC} ($\mu\text{A}/\text{cm}^2$)	Light source
³² Pt/BFO/SRO/STO	8.7	0.18	Halogen lamp
³³ Pt/BFO/LSMO/STO	16.6	0.1	Halogen lamp
³⁴ Pt/Fe/BFO/LSMO/STO	21	0.6	Halogen lamp
³⁵ Au/PLZT/Nb:STO	39.4	0.025	UV source
^a Au/BZT-BCT/Nb:STO	32.8	3.5	Xe lamp

^aThe present work

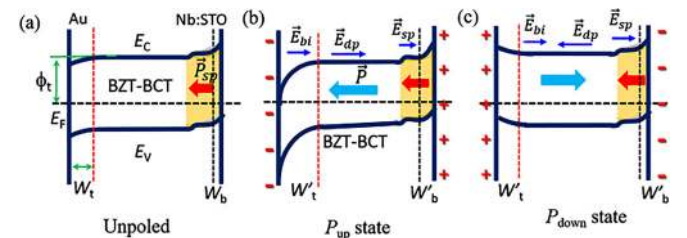


FIG. 5. Schematic energy band diagram of the Au/BZT-BCT/Nb:STO heterostructure in (a) unpoled, (b) P_{up} state, and (c) P_{down} states. The ϕ_t is the Schottky barrier height at the top interface. The E_C , E_V , and E_F are the conduction band minimum, valence band maximum, and the Fermi level, respectively. The W_t and W_b represent the barrier width at the top and bottom interfaces, respectively.

The photo-current response with respect to time under light ON and OFF states is recorded for the Au/BZT-BCT/Nb:STO sample at the zero bias condition. The result is plotted in Fig. 4(b). The plot shows a quick photo-current response under both light ON and OFF states. To study the stability of photovoltage and photocurrent, the V_{OC} and J_{SC} recorded under the light ON state as a function of time are displayed in Fig. 4(c) and in the inset, respectively. The figure shows that the V_{OC} and J_{SC} values are indeed stable for a longer duration of time. To understand the light intensity effect on the PV response, the J - V curves are measured at 60, 80, and 100 mW/cm² light intensities and the respective plots are shown in Fig. 4(d). Interestingly, the plots reveal an increase in J_{sc} with increase in light intensities without showing a significant change in V_{oc} .

In summary, the ferroelectric 0.5Ba(Zr_{0.2}Ti_{0.8})O₃-0.5(Ba_{0.7}Ca_{0.3})TiO₃ film was fabricated on a (001)Nb:SrTiO₃ substrate by the pulsed laser deposition technique for the photovoltaic studies. The film was grown along (00 l) epitaxial orientation with a large compressive misfit strained (2.3%) state. The Au/BZT-BCT/Nb:STO film displayed a P - E hysteresis loop with a large imprint effect. The non-switchable preferentially oriented domains due to the flexoelectric effect and interfacial p-n junction are envisaged to be the reason for the imprint phenomenon. The PFM switching studies demonstrated that the domains are indeed oriented in a preferred direction with non-switchable character which leads to the strong self-polarization effect. It is noteworthy to mention that the BZT-BCT film exhibits a poling directional dependent large photovoltaic response with a maximum V_{OC} value of 1.1 V. The observed photo-response is the consequence of the net internal field associated with the depolarization field along with an additional contribution from the self-polarization effect. Hence, the large and stable photovoltaic characteristics of the BZT-BCT film give an additional dimension to the multifunctional materials with a huge application potential in the field of optoelectronics related devices.

See [supplementary material](#) for the surface topography and the line scan of the surface profilometry recorded on the film.

¹J. F. Scott and C. A. Paz de Araujo, *Science* **246**, 1400 (1989).

²B. H. Park, B. S. Kang, S. D. Bu, T. W. Noh, J. Lee, and W. Jo, *Nature* **401**, 682 (1999).

³P. Maksymovych, S. Jesse, P. Yu, R. Ramesh, A. P. Baddorf, and S. V. Kalinin, *Science* **324**, 1421 (2009).

⁴Z. Wang, W. Zhao, W. Kang, A. B. Khelladi, Y. Zhang, Y. Zhang, J. O. Klein, D. Ravelosona, and C. Chappert, *J. Phys. D: Appl. Phys.* **47**, 045001 (2014).

⁵D. S. Jeong, R. Thomas, R. S. Katiyar, J. F. Scott, H. Kohlstedt, A. Petraru, and C. S. Hwang, *Rep. Prog. Phys.* **75**, 76502 (2012).

⁶V. Annapureddy, H. Palneedi, G.-T. Hwang, M. Peddigari, D.-Y. Jeong, W.-H. Yoon, K.-H. Kim, and J. Ryu, *Sustainable Energy Fuels* **1**, 2039 (2017).

⁷S. Y. Yang, J. Seidel, S. J. Byrnes, P. Shafer, C. H. Yang, M. D. Rossell, P. Yu, Y. H. Chu, J. F. Scott, J. W. Ager, L. W. Martin, and R. Ramesh, *Nat. Nanotechnol.* **5**, 143 (2010).

⁸M. Yang, A. Bhatnagar, and M. Alexe, *Adv. Electron. Mater.* **1**, 1500139 (2015).

⁹Y. Yuan, Z. Xiao, B. Yang, and J. Huang, *J. Mater. Chem. A* **2**, 6027 (2014).

¹⁰C. Paillard, X. Bai, I. C. Infante, M. Guennou, G. Geneste, M. Alexe, J. Kreisel, and B. Dkhil, *Adv. Mater.* **28**, 5153 (2016).

¹¹K. T. Butler, J. M. Frost, and A. Walsh, *Energy Environ. Sci.* **8**, 838 (2015).

¹²V. M. Fridkin and B. N. Popov, *Sov. Phys. Usp.* **126**, 657 (1978).

¹³W. T. H. Koch, R. Munser, W. Ruppel, and P. Wurfel, *Solid State Commun.* **17**, 847 (1975).

¹⁴P. Poosanaas and K. Uchino, *Mater. Chem. Phys.* **61**, 36 (1999).

¹⁵X. Yang, X. Su, M. Shen, F. Zheng, Y. Xin, L. Zhang, M. Hua, Y. Chen, and V. G. Harris, *Adv. Mater.* **24**, 1202 (2012).

¹⁶W. Liu and X. Ren, *Phys. Rev. Lett.* **103**, 257602 (2009).

¹⁷J. K. Li, C. Ge, K. J. Jin, J. Y. Du, J. T. Yang, H. Bin Lu, and G. Z. Yang, *Appl. Phys. Lett.* **110**, 142901 (2017).

¹⁸N. Ma, K. Zhang, and Y. Yang, *Adv. Mater.* **29**, 1703694 (2017).

¹⁹A. B. Swain, V. Subramanian, and P. Murugavel, *Ceram. Int.* **44**, 6861 (2018).

²⁰K. Brajesh, K. Tanwar, M. Abebe, and R. Ranjan, *Phys. Rev. B* **92**, 224112 (2015).

²¹Y. Noguchi, H. Maki, Y. Kitanaka, H. Matsuo, and M. Miyayama, *Appl. Phys. Lett.* **113**, 012903 (2018).

²²P. V. Yudin and A. K. Tagantsev, *Nanotechnology* **24**, 432001 (2013).

²³H. S. Kim, C. R. Lee, J. H. Im, K. B. Lee, T. Moehl, A. Marchioro, S. J. Moon, R. Humphry-Baker, J. H. Yum, J. E. Moser, M. Grätzel, and N. G. Park, *Sci. Rep.* **2**, 591 (2012).

²⁴Z. Tan, J. Tian, Z. Fan, Z. Lu, L. Zhang, D. Zheng, Y. Wang, D. Chen, M. Qin, M. Zeng, X. Lu, X. Gao, and J. M. Liu, *Appl. Phys. Lett.* **112**, 152905 (2018).

²⁵M. G. Han, M. S. J. Marshall, L. Wu, M. A. Schofield, T. Aoki, R. Twisten, J. Hoffman, F. J. Walker, C. H. Ahn, and Y. Zhu, *Nat. Commun.* **5**, 4693 (2014).

²⁶Y. Saya, S. Watanabe, M. Kawai, H. Yamada, and K. Matsushige, *Jpn. J. Appl. Phys.* **39**, 3799 (2000).

²⁷Y. Zhou, H. K. Chan, C. H. Lam, and F. G. Shin, *J. Appl. Phys.* **98**, 024111 (2005).

²⁸B. C. Jeon, D. Lee, M. H. Lee, S. M. Yang, S. C. Chae, T. K. Song, S. D. Bu, J. S. Chung, J. G. Yoon, and T. W. Noh, *Adv. Mater.* **25**, 5643 (2013).

²⁹J. Chen, Y. Luo, X. Ou, G. Yuan, Y. Wang, Y. Yang, J. Yin, and Z. Liu, *J. Appl. Phys.* **113**, 204105 (2013).

³⁰D. Lee and T. W. Noh, *Philos. Trans. R. Soc. A* **370**, 4944 (2012).

³¹D. Lee, A. Yoon, S. Y. Jang, J.-G. Yoon, J.-S. Chung, M. Kim, J. F. Scott, and T. W. Noh, *Phys. Rev. Lett.* **107**, 057602 (2011).

³²D. Lee, S. H. Baek, T. H. Kim, J. G. Yoon, C. M. Folkman, C. B. Eom, and T. W. Noh, *Phys. Rev. B* **84**, 125305 (2011).

³³L. You, F. Zheng, L. Fang, Y. Zhou, L. Z. Tan, Z. Zhang, G. Ma, D. Schmidt, A. Rusydi, L. Wang, L. Chang, A. M. Rappe, and J. Wang, *Sci. Adv.* **4**, 3438 (2018).

³⁴R. Guo, L. You, Y. Zhou, Z. Shihui Lim, X. Zou, L. Chen, R. Ramesh, and J. Wang, *Nat. Commun.* **4**, 1990 (2013).

³⁵M. Qin, K. Yao, and Y. C. Liang, *J. Appl. Phys.* **105**, 061624 (2009).

³⁶Z. Lu, P. Li, J. G. Wan, Z. Huang, G. Tian, D. Pan, Z. Fan, X. Gao, and J. M. Liu, *ACS Appl. Mater. Interfaces* **9**, 27284 (2017).

³⁷W. Dong, Y. Guo, B. Guo, H. Li, H. Liu, and T. W. Joel, *ACS Appl. Mater. Interfaces* **5**, 6925 (2013).

³⁸Z. Xi, J. Ruan, C. Li, C. Zheng, Z. Wen, J. Dai, A. Li, and D. Wu, *Nat. Commun.* **8**, 15217 (2017).

³⁹L. Zhao, Z. Lu, F. Zhang, G. Tian, X. Song, Z. Li, K. Huang, Z. Zhang, M. Qin, S. Wu, X. Lu, M. Zeng, X. Gao, J. Dai, and J. M. Liu, *Sci. Rep.* **5**, 9680 (2015).